An Accurate Semi-Analytical Framework for Full-Chip TSV-induced Stress Modeling

Yang Li David Z. Pan

Department of Electrical and Computer Engineering
The University of Texas at Austin
jerryyangli@gmail.com dpan@ece.utexas.edu

Abstract

TSV-induced stress is an important issue in 3D IC design since it leads to serious reliability problems and influences device performance. Existing finite element method can provide accurate analysis for the stress of simple TSV placement, but is not scalable to larger designs due to its expensive memory consumption and high run time. On the contrary, linear superposition method is efficient to analyze stress in full-chip scale, but sometimes it fails to provide an accurate estimation since it neglects the stress induced by interactions between TSVs. In this paper we propose an accurate two-stage semi-analytical framework for full-chip TSV-induced stress modeling. In addition to the linear superposition, we characterize the stress induced by interactions between TSVs to provide more accurate full-chip modeling. Experimental results demonstrate that the proposed framework can significantly improve the accuracy of linear superposition method with reasonable overhead in run time.

Categories and Subject Descriptors

B.7.2 [*Hardware, Integrated Circuits*]: Design Aids

General Terms

Design

Keywords

3D IC, TSV, stress, analytical model

1. Introduction

Through-silicon-via (TSV) induces thermo-mechanical stress during the fabrication process and operation phase of 3D IC due to the mismatch of coefficients of thermal expansion (CTE) between the materials of TSV and substrate. The thermo-mechanical stress further induces mobility variation and influences the device performance [1, 2], and may cause serious reliability issues like crack growth in the chip [3, 4]. Hence, it is important to accurately analyze the TSV-induced stress in the design phase in order to predict circuit performance and avoid reliability issues. Most previous works on thermo-mechanical stress employ finite element method (FEM) to characterize the stress [5–7]. While FEM can accurately analyze the stress of simple TSV placement, it encounters enormous difficulties when tackling larger design due to its expensive memory consumption and high run time. To overcome the difficulties of FEM, some analytical methods have been proposed [3, 8]. Although these analytical methods are generally efficient, they usually assume an over-simplified TSV structure and sometimes lead to results with unacceptable error [9].

Besides FEM and analytical methods, linear superposition method has been proposed in [9–11] to both consider realistic TSV structure and complete the simulation within reasonable run time and memory usage. The fundamental idea of linear superposition method is to calculate the stress contribution of each TSV separately, and then superpose them. However, when calculating the stress contribution of a certain TSV, linear superposition method assumes the TSV is a single one in isolation and neglects the influence of nearby TSVs. This assumption neglects the fact that nearby TSVs have different mechanical properties compared with substrate and will behave differently, and therefore they have considerable influences on stress contribution of the TSV. We term the stress induced by the interactions between TSVs *interactive stress*. Since linear superposition method fails to characterize interactive stress, its accuracy will suffer with high TSV integration density.

To overcome the limitations of previous works, we propose in this paper an accurate semi-analytical framework for full-chip TSV-induced stress modeling. The proposed framework uses complex variable method in elasticity to characterize the interactive stress between TSVs, and achieves an analytical solution to it. Based on the analytical solution, the proposed framework calculates the interactive stress for each simulation point on chip, and uses it to adjust the analysis result of linear superposition method. Experimental results demonstrate the proposed framework significantly benefits the accuracy of linear superposition method under short additional run time. For example, in a placement consisting of two baseline TSVs with 8um pitch, the proposed framework reduces the average error rate of linear superposition from 36.8% to 14.3% in the region surrounding TSVs with only 1% additional run time.

The main contributions of this paper include the following: (1) For the first time, the paper proposes the concept of interactive stress, analyzes its mechanism and points out its importance to stress modeling. (2) The paper shows that the existing linear superposition method will induce more error when the pitch between TSVs decreases due to the neglect of interactive stress. (3) The paper applies the complex variable method in elasticity to interactive stress, and proposes an analytical solution. (4) The paper proposes a semi-analytical framework which can accurately characterize the TSV-induced stress in full-chip scale within reasonable run time and memory usage.

The rest of paper is organized as follows. In Section 2, we will first introduce the baseline TSV structure and stress simulation methodology used in the paper. Then we will define and analyze the interactive stress between TSVs, and point out its importance for stress modeling. In Section 3, we will first propose a 2D analytical stress model for a single TSV which considers the influence of liner on stress field. And then we apply the complex variable method in elasticity to characterize the interactive stress. In Section 4, based on the analytical solution to interactive stress, we will propose an accurate semi-analytical framework for full-chip TSV-induced stress modeling. In Section 5, we will validate our proposed framework on several placements, and justify its accuracy and scalability. Conclusions are drawn in Section 6. More details of the theory and experimental results can be found in Appendix.

Permission to make digital or hard copies of all or part of this work for personal or classroom use is granted without fee provided that copies are not made or distributed for profit or commercial advantage and that copies bear this notice and the full citation on the first page. To copy otherwise, to republish, to post on servers or to redistribute to lists, requires prior specific permission and/or a fee.
DAC '13, May 29 - June 07 2013, Austin, TX, USA
Copyright © 2013 ACM 978-1-4503-2071-9/13/05…$15.00

2. Preliminary

2.1 Baseline TSV Structure and Stress Simulation

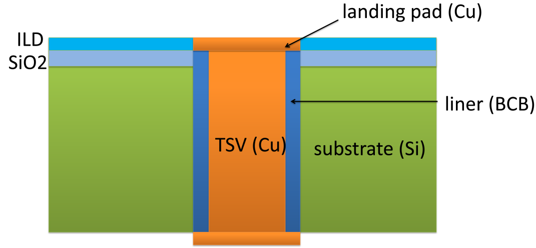

Figure 1. A typical TSV structure.

Various TSV structures have been reported in previous literature [9, 12, 13]. Our baseline TSV structure shown in Figure 1 is based on a typical one [9]. In the structure, TSV consists of copper TSV body and a benzocyclobutene (BCB) liner. We validate our proposed framework on the baseline TSV structure. However, we also use SiO2 as an alternative liner material and test the proposed framework on it (Appendix A.2).

We use commercial FEM tool to obtain the golden result of the stress simulation. In our FEM simulation, the entire structure is assumed to be linear elastic and isotropic with constant material properties. We also assume it is stress free at the annealing temperature, and bears a -250K thermal load during the annealing process.

2.2 Mechanism of Interactive Stress

Interactive stress is defined as the stress induced by the interactions between TSVs due to the mismatch of mechanical properties (Young's modulus and Poisson's ratio) of TSV body, liner and substrate. Here we use a placement consisting of two TSVs to illustrate how interactive stress originates (Figure 2). To simplify the problem, we consider one TSV as the aggressive TSV, and the other as the victim, and then vice versa. In the stress field induced by the aggressive TSV, the victim TSV just acts as a part of medium with different mechanical material properties from substrate.

If we assume victim TSV has the same mechanical property as substrate, the stress field of entire placement is the same as that of a single TSV in isolation. Under this circumstance, we term the stress field of entire placement *ideal stress distribution*, term the stress load along the boundary Γ_1 between the victim and substrate *ideal stress load* and term the deformation of the victim and surrounding substrate *ideal deformation*. However, in reality, the stress load along the boundary Γ_1 must be different from ideal stress load. Otherwise surrounding substrate will deform as ideal deformation, but the victim will deform more significantly than ideal deformation since Young's modulus of TSV is smaller than that of substrate, hence under the same stress load, victim TSV will deform more significantly. In that sense, if the stress load along the boundary Γ_1 does not change, there will be some overlap or discrepancy between victim TSV and substrate, which definitely cannot happen in reality. Interactive stress just originates from the change of stress load along the boundary Γ_1 . And then, interactive stress will propagate into the substrate and TSV, and influence the stress distribution in these regions.

Linear superposition method [9] neglects the existence of victim TSV when considering the stress contribution of aggressive TSV, and thus fails to consider interactive stress induced by the interaction between TSVs. For the TSV structure with SiO2 liner, interactive stress is not very severe due to a smaller Young's modulus difference between liner and substrate materials. And hence the linear superposition method can achieve acceptable accuracy though our proposed framework can still significantly improve the accuracy of stress analysis. However, the interactive stress is considerable for the TSV structure with BCB liner due to a much bigger Young's modulus difference between liner and substrate materials. Figure 3 shows the device layer distribution of stress component σ_{xx} calculated by FEM and linear superposition method

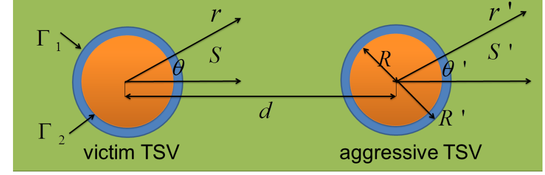

Figure 2. Illustrations for the characterization of interactive stress.

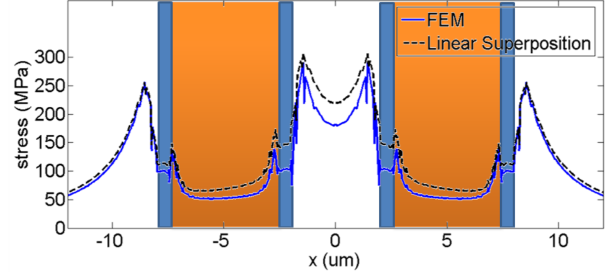

Figure 3. Comparison between FEM and linear superposition method on σ_{xx} distribution along the line through the centers of two TSVs.

along the line through the centers of two baseline TSVs. If we assume FEM simulation contains negligible errors, the discrepancy of results is totally caused by interactive stress. In this figure, we can see linear superposition method overestimates stress level generally, and leads the analysis to an error rate as high as 50% in some regions of interests. Therefore, it is very necessary to consider and characterize interactive stress.

The key points to characterize interactive stress lay in two aspects. One is how to decouple the interaction between aggressive and victim TSV; the other one is how to achieve equilibrium state between the deformation of TSV body, liner and substrate. Firstly, interactive stress originates from the victim TSV under the stress field of the aggressive, but reversely influences the deformation of the aggressive. The influenced deformation might in turn change the stress field of the aggressive, and lead to the change of interactive stress. Therefore, it is important to decouple the interaction between TSVs. Secondly, we need to investigate what is the smart stress load of victim TSV that ensures TSV body, liner and substrate deform harmonically and prevents the occurrence of overlap or discrepancy between these regions.

3. Analysis of Interactive Stress

In this section, we analyze and characterize the interactive stress. We first introduce the basics of elasticity theory which serves as the fundamental of derivation. Then we propose a 2D analytical stress model for a single TSV which has considered the influence of liner on stress field. This model can be used as the ideal stress distribution induced by the aggressive TSV. Based on this model, we employ the complex variable method in elasticity to characterize the interactive stress.

3.1 Basics of Elasticity Theory

Elasticity theory generally uses a second-order tensor to represent the stress in solids. For example, in a 3D problem, a second-order stress tensor is shown as (1).

$$\sigma = \begin{bmatrix} \sigma_{11} & \sigma_{12} & \sigma_{13} \\ \sigma_{21} & \sigma_{22} & \sigma_{23} \\ \sigma_{31} & \sigma_{32} & \sigma_{33} \end{bmatrix} \quad (1)$$

In this tensor, the first subscript of each component represents the normal direction of plane the stress component aims at. The second subscript represents the direction of component. In a 3D Cartesian coordinate system, index 1,2,3 represent index x,y,z respectively; while in a cylindrical coordinate system, they represent index r,θ,and z. The stress tensor is generally symmetric.

Since stress tensor and other tensors (like strain tensor) can be represented in various coordinate systems, it is necessary to introduce how to transform tensors between different coordinate systems. If the

original and new coordinate system are respectively cylindrical and Cartesian system, the transform matrix and transform formula is shown as (2).

$$Q = \begin{bmatrix} \cos\theta & -\sin\theta & 0 \\ \sin\theta & \cos\theta & 0 \\ 0 & 0 & 1 \end{bmatrix}, \qquad \sigma_{xyz}=Q\cdot\sigma_{r\theta z}\cdot Q^T \tag{2}$$

where $\sigma_{r\theta z}$ and σ_{xyz} are stress tensors respectively in the cylindrical and Cartesian coordinate system; θ is the angle between x-axis of the Cartesian system and r-axis of the cylindrical system.

When we focus on the stress on the surface of solids, we can simplify the problem into a 2D problem. In a 2D problem, we only consider the stress component σ_{rr}, $\sigma_{r\theta}$ and $\sigma_{\theta\theta}$. Other components are either null or combinations of these components. Since the key issue of this paper is to characterize the interactive stress in device layer, it is reasonable to analyze the interactive stress using the complex variable method in elasticity for 2D problems [14]. In the complex variable method, the pursuit of stress tensor is transformed to the pursuit of two analytical functions ϕ and ψ (in complex analysis meanings) which satisfy the boundary condition. These two analytical functions are termed complex potential. If complex potentials are successfully obtained, stress tensor and displacement vector can be achieved through (3 - 5).

$$\sigma_{rr} + \sigma_{\theta\theta} = 2[\phi'(z) + \overline{\phi'(z)}] \tag{3}$$

$$\sigma_{\theta\theta} - \sigma_{rr} + 2i\sigma_{r\theta} = 2\exp(2i\theta)[\bar{z}\phi''(z) + \psi'(z)] \tag{4}$$

$$u_r + iv_\theta = \frac{1+v}{E}\exp(-i\theta)[\frac{3-v}{1+v}\phi(z) - z\overline{\phi'(z)} - \overline{\psi(z)}] \tag{5}$$

where z represents the position of the point $(r,\ \theta)$ in the complex plane, $z = r\exp(i\theta)$; u_r and v_θ are displacement of the point $(r,\ \theta)$ in r-direction and θ-direction; $\phi(z)$ and $\psi(z)$ are complex potentials; E and v are Young's modulus and Poisson's ratio of corresponding materials.

3.2 Stress Field induced by the Aggressive TSV

In this section, we propose a 2D analytical stress model for a single TSV. The model can be used to represent the stress field induced by the aggressive TSV. As what is shown in [9, 15], liner has considerable influences on the stress field of TSV. Hence, different from previous 2D analytical models, the proposed model incorporates the influence of liner into its derivation. It can be applicable to liner with any material and thickness. In this model, as we focus on the stress of device layer, plane stress condition is assumed. Although it is a 2D model, it provides a simple while accurate enough basis to characterize interactive stress since interactive stress is kind of a second order effect of the original stress field. Due to the page limit, we omit the derivation of model, and directly give the formula for the stress field in the substrate shown in (6). We adopt the cylindrical coordinate system S' (Figure 2).

$$\sigma_{rr}\mid_{ideal} = \frac{K}{r'^2} \qquad \sigma_{\theta\theta}\mid_{ideal} = -\frac{K}{r'^2} \qquad \sigma_{r\theta}\mid_{ideal} = 0, \quad r' > R' \tag{6}$$

where R' is the radius of TSV; r' is the distance between the simulation point and the center of TSV; K is a constant which can be directly calculated from the material property and geometry specification of TSV structure (Appendix A.4); $\sigma_{rr}\mid_{ideal}$, $\sigma_{\theta\theta}\mid_{ideal}$ and $\sigma_{r\theta}\mid_{ideal}$ are stress components. The formula shows stress components decrease with r'^{-2} in the substrate.

Since we will take advantage of the boundary condition along Γ_1 (Figure 2) to derive the interactive stress, we replace the current coordinate system with the cylindrical coordinate system S (Figure 2), and factorize the following stress combination along Γ_1 based on (6). We omit the derivation and give the result in (7). The corresponding displacement combination factorized along Γ_1 is shown in (8).

$$(\sigma_{rr} - i\sigma_{r\theta})\mid_{\Gamma_1,ideal} = \sum_{m=2}^{\infty}\frac{K(m-1)}{R'^2}(\frac{R}{d})^m\exp(im\theta) \tag{7}$$

$$(u_r + iv_\theta)\mid_{\Gamma_1,ideal} = \sum_{m=-\infty}^{\infty}\frac{K}{R'}\frac{1+v_s}{E_s}(\frac{d}{R'})^m\exp(im\theta) \tag{8}$$

In (7) and (8), u_r and v_θ represents the displacement in r-direction and θ-direction; d is the pitch between TSVs; E_s and v_s are the Young's modulus and Poisson's ratio of silicon. (7) and (8) are the ideal stress distribution and displacement field factorized along Γ_1. In next section, we will investigate how they change in reality, and use them to derive the interactive stress.

3.3 Characterization of Interactive Stress

To characterize the interactive stress, we need to decouple interactions between TSVs, and establish an equilibrium state between the deformation of TSV body, liner and substrate. Similar to previous analysis, for a TSV pair, we consider one as the aggressive and the other one as the victim in one round, and then vice versa in another round. In each round, we observe the phenomenon that the interactive stress between the aggressive and victim TSV has little influence on the stress field around aggressive TSV (Details can be referred to Appendix A.1). It infers that the boundary condition around the aggressive can be ignored. Specifically, we can just consider the stress induced by the reaction of victim under the stress field of aggressive, and ignore the influence of such reaction on the deformation of aggressive. In this way, we avoid iterations of interaction between the stress field of aggressive and victim TSV, and thus decouple the interactions between them.

We use the complex variable method in elasticity to achieve the equilibrium state between the deformation of victim TSV and substrate. The general flow is as follows. First, we adopt the method of undetermined coefficients, and assume a general form of complex potentials in TSV body, liner and substrate respectively. We also assume a stress load along the boundary of victim TSV. Second, we investigate how victim TSV and substrate deform under this stress load, and establish the relations of assumed complex potentials to the assumed stress load. Finally, based on the boundary condition between victim TSV and substrate, we solve the assumed stress load and obtain the analytical solution to interactive stress. Section 3.3.1 and 3.3.2 respectively investigate how substrate and victim TSV deforms under the assumed stress load. Section 3.3.3 solves the assumed stress load and obtains the solution to interactive stress.

3.3.1 Elasticity Analysis of Substrate

In this section we investigate how substrate deforms under a certain stress load. The stress load that the substrate bears comes from two parts. One is from the boundary of aggressive TSV; the other one is from the boundary of victim TSV. The stress load along the boundary of the aggressive is almost known. But the stress load along the boundary of the victim is unknown. Therefore, we need to find a general relation of substrate deformation to arbitrary stress load along the boundary of the victim. Additionally, the non-uniform distribution of stress load along the boundary of the victim also increases the difficulty of solution.

To tackle the problem, we decompose the stress load along the boundary Γ_1 into two parts $\hat{f}_0$ and $\hat{f}_1$, where $\hat{f}_0$ is the ideal stress load defined in Section 3.2, $\hat{f}_1$ is the change of ideal stress load along Γ_1 in reality. In section 3.2, we have obtained $\hat{f}_0$ and corresponding displacement of substrate under the stress field of aggressive TSV and $\hat{f}_0$, and factorize them along the boundary Γ_1 shown in (7) and (8). Hence, we only need to further investigate how the substrate deforms under $\hat{f}_1$, and then superpose them to obtain the deformation of substrate in reality. Since $\hat{f}_1$ is unknown, we represent it as a series factorized along Γ_1 in (9).

$$\sigma_{rr} - i\sigma_{r\theta}\mid_{\Gamma_1,change} = \sum_{m=-\infty}^{\infty} f_m\exp(im\theta) \tag{9}$$

where $f_m$are undermined coefficients. We will continue to see how the substrate deforms under this assumed stress load.

To investigate the deformation of substrate under $\hat{f}_1$, we assume the corresponding complex potentials in the region of substrate. Based on the fact that the interactive stress has little influence on the stress field around the aggressive TSV (Appendix A.1), we ignore the boundary condition of aggressive TSV, and consider the substrate as pure silicon. Therefore, according to the theory of complex analysis, complex potentials $\phi_s(z)$ and $\psi_s(z)$, which are analytical functions in an infinite region containing a circular hole, can be further represented as a series in the complex plane as (10).

$$\phi_s'(z) = \sum_{m=-\infty}^{0} A_{s,m}z^m \qquad \psi_s'(z) = \sum_{m=-\infty}^{0} B_{s,m}z^m \tag{10}$$

where $\phi_s'(z)$and$\psi_s'(z)$are derivatives of $\phi_s(z)$ and $\psi_s(z)$; $A_{S,m}$ and $B_{s,m}$ are undetermined coefficients; z represents the position of simulation point in the complex plane. We can further adapt these complex potentials to the stress load in (9) to determine the unknown coefficients of complex potentials, and then achieve the displacement of substrate under the assumed stress load.

Based on (3 - 5) and (9 - 10), we can achieve the displacement field $(u_r + iv_\theta)\ |_{change}$ under the stress load $\hat{f}_1$. Then we superpose it with the displacement field $(u_r + iv_\theta)\ |_{ideal}$ under ideal stress load $\hat{f}_0$ and the stress load of aggressive TSV, and obtain the displacement field of substrate $(u_r + iv_\theta)\ |_{substrate}$. Specifically, the displacement along the boundary Γ_1 will be

$$(u_r + iv_\theta)\ |_{\Gamma_1,substrate} = (u_r + iv_\theta)\ |_{\Gamma_1,ideal} + (u_r + iv_\theta)\ |_{\Gamma_1,change} \quad (11)$$

We will further use the displacement field of substrate obtained from (11) to fit the displacement field of TSV to determine the assumed stress load along the boundary Γ_1 .

3.3.2 Elasticity Analysis of TSV

In this section, we investigate how TSV body and liner deforms under the assumed stress load $\hat{f}_0 + \hat{f}_1$. This problem encounters even more complexity than the previous one since the mechanical properties of TSV body and liner are generally different, and we need to preserve an equilibrium state between their deformation under arbitrary stress load.

To tackle this problem, we assume different complex potentials for TSV body and liner, and take advantage of the boundary condition between TSV body and liner to establish their relationship. After that we try to find their relation to the assumed stress load. Specifically, since the region of TSV body is circular and the region of liner is ring, according to the theory of complex analysis, the complex potentials of TSV body $\phi_c(z)$ and$\psi_c(z)$, and the complex potentials of liner$\phi_l(z)$and $\psi_l(z)$ can be assumed to be

$$\phi_c'(z) = \sum_{m=0}^{\infty} A_{c,m} z^m \qquad \psi_c'(z) = \sum_{m=0}^{\infty} B_{c,m} z^m \quad (12)$$

$$\phi_l'(z) = \sum_{m=-\infty}^{\infty} A_{l,m} z^m \quad \psi_l'(z) = \sum_{m=-\infty}^{\infty} B_{l,m} z^m \quad (13)$$

where $\phi_c'(z)$, $\psi_c'(z)$, $\phi_l'(z)$ and $\psi_l'(z)$ are the derivatives of $\phi_c(z)$, $\psi_c(z)$, $\phi_l(z)$ and $\psi_l(z)$; $A_{c,m}$, $B_{c,m}$, $A_{l,m}$and $B_{l,m}$ are undetermined coefficients. We adapt these assumed complex potentials to the boundary condition along Γ_1 and Γ_2, and obtain the corresponding displacement field within TSV.

Specifically, these complex potentials need to satisfy the boundary condition along Γ_1 and Γ_2. In details, they should satisfy the continuous condition of stress component combination along Γ_1 and Γ_2 shown as (14) and (15), and satisfy the continuous condition of displacement along Γ_2 shown as (16).

$$\begin{aligned}\sigma_{rr} - i\sigma_{r\theta}\ |_{\Gamma_1,liner} = & \sum_{m=2}^{\infty} \frac{K(m-1)}{R'^2} (\frac{R'}{d})^m \exp(im\theta) \\ & + \sum_{m=-\infty}^{\infty} f_m \exp(im\theta)\end{aligned} \quad (14)$$

$$\sigma_{rr} - i\sigma_{r\theta}\ |_{\Gamma_2,liner} = \sigma_{rr} - i\sigma_{r\theta}\ |_{\Gamma_2,copper} \quad (15)$$

$$(u_r + iv_\theta)\ |_{\Gamma_2,liner} = (u_r + iv_\theta)\ |_{\Gamma_2,copper} \quad (16)$$

Based on (3 - 5) and (12 - 16), we obtain the displacement field in TSV body and liner $(u_r + iv_\theta)\ |_{copper}$ and $(u_r + iv_\theta)\ |_{liner}$. We will establish an equilibrium state between the displacement field of liner $(u_r + iv_\theta)\ |_{liner}$ and that of substrate $(u_r + iv_\theta)\ |_{\Gamma_1,substrate}$ to determine the stress load along Γ_1 in next section.

3.3.3 Analytical Solution to Interactive Stress

After finishing the elasticity analysis of substrate and TSV, we obtain the displacement field within TSV and silicon. We further take advantage of the continuous condition of displacement along the boundary $\Gamma_1$and obtain (17).

$$(u_r + iv_\theta)\ |_{\Gamma_1,substrate} = (u_r + iv_\theta)\ |_{\Gamma_1,liner} \quad (17)$$

Algorithm 1 Full-chip TSV-induced stress modeling framework.

Input: TSV list, stress library
Output: stress map

Stage I Linear Superposition Method (Table Look-up Method)
```
for each simulation point p
    find nearby TSVs;
    for each nearby TSV of p
        calculate stress contribution;
        add it to p.linear;
    end
end
```

Stage II Interactive Stress Calculation (Analytical Method)
```
for each simulation point p
    find nearby TSV pairs;
    for each nearby TSV pair of p
        calculate interactive stress contribution using (18);
        convert the interactive stress contribution using (2);
        add it to p.interactive;
    end
end
```

Final:
```
for each simulation point p
    stress tensor p.stress ← p.linear + p.interactive (tensor addition);
end
```

Up to now, all the necessary equations have been established. Based on (3 - 5) and (7 - 17), we can solve the problem, and achieve the ultimate analytical solution to the interactive stress represented in the coordinate system S (Figure 2) shown in (18) .

$$\begin{aligned}\sigma_{rr} = & \frac{K}{R'^2} \sum_{m=2}^{\infty} \cos(m\theta) \left[\left(\frac{r}{d}\right)^m \left(h_{i1}(m) - \frac{R'^2}{r^2} h_{i2}(m) \right) \right. \\ & \left. + \left(\frac{R'^2}{rd}\right)^m \left(h_{i3}(m) - \frac{R'^2}{r^2} h_{i4}(m) \right) \right] \\ \sigma_{\theta\theta} = & \frac{K}{R'^2} \sum_{m=2}^{\infty} \cos(m\theta) \left[\left(\frac{r}{d}\right)^m \left(h_{i5}(m) + \frac{R'^2}{r^2} h_{i2}(m) \right) \right. \\ & \left. + \left(\frac{R'^2}{rd}\right)^m \left(h_{i6}(m) + \frac{R'^2}{r^2} h_{i4}(m) \right) \right] \\ \sigma_{r\theta} = & \frac{K}{R'^2} \sum_{m=2}^{\infty} \sin(m\theta) \left[\left(\frac{r}{d}\right)^m \left(h_{i7}(m) + \frac{R'^2}{r^2} h_{i2}(m) \right) \right. \\ & \left. + \left(\frac{R'^2}{rd}\right)^m \left(h_{i8}(m) - \frac{R'^2}{r^2} h_{i4}(m) \right) \right]\end{aligned} \quad (18)$$

where r, θ are the position of simulation point in the coordinate system S; $h_{ij}(m)$, $i = 1, 2, 3$, $j = 1, 2, \ldots, 8$, are functions which only depend on material properties and geometry specification of TSV, and are irrelevant to TSV placement (Appendix A.4). In (18), if $r < R$ (TSV body), $i = 1$, $h_{1j} = 0$, $j = 3, 4, 6, 8$; if $R < r < R'$(liner), $i = 2$; if $r > R'$(substrate), $i = 3$, $h_{ij} = 0$, $j = 1, 2, 5, 7$.

In the above analytical solution, it is not hard to see each term of the solution generally decreases with a speed no slower than (R'/d) as m increases. Since $R'/d < 0.5$, the series will converge with a reasonable amount of terms. We employ 9 terms in practice ($m_{max} = 10$).

4. Full-Chip Stress Modeling Framework

In this section, we propose an interactive stress aware two-stage semi-analytical framework for full-chip TSV-induced stress modeling as shown in Algorithm 1. The first stage performs linear superposition [9] to obtain a rough stress estimation. Since stress decays to a negligible intensity after a certain distance from TSV, the framework only considers the stress induced by nearby TSVs, and ignores other TSVs' contribution in order to improve the efficiency of algorithm. Hence, in Stage I, we firstly determine what are the nearby TSVs for each simulation point. Here, we consider a TSV with distance less than a certain value (e.g. 25um) from the simulation point as nearby TSV. After that, we employ a table look-up method to find the stress contribution of nearby TSVs and superpose them for each simulation point. The com-

plexity of first stage is $O(n)$, where n is the amount of simulation points.

The second stage calculates interactive stress for each simulation point. The general idea is to first calculate the interactive stress contribution of each TSV pair, and then superpose them together. Since a certain TSV may interact with multiple TSVs and each induces interactive stress, during the calculation, a TSV may form multiple pairs with other TSVs. For each TSV pair, although there may exist other TSVs nearby the pair and make the substrate not as pure silicon, we can still use the analytical formula derived in Section 3.3. This is because of the fact that the interactive stress induced by the interaction of a TSV pair is nearly irrelevant to the existence of other TSVs nearby the pair (Details can be referred to Appendix A.1).

Similar to the first stage, the second stage only considers the interactive stress contribution of nearby TSV pairs, and firstly determines what are the nearby pairs for each simulation point. Here, we consider any two TSVs as a nearby pair for a certain point if the pair satisfies 1) the pitch of pair is within a certain distance (e.g. 25um) and 2) the victim TSV is located within a certain distance (e.g. 25um) from the point. For a TSV pair, if the pitch is large, the interactive stress will become too small to be considered. For a simulation point, since interactive stress decreases no slower than r^{-2} (Section 3.3), r is the distance from the victim TSV to the point, if the distance is too large, we can ignore the interactive stress contribution of the pair in one round to the point. Please note in a TSV pair, a TSV can both become aggressive and victim in two rounds. Therefore, although a TSV pair may not become nearby pair for a simulation point in one round due to the large distance from the victim to the point, when the roles of TSVs exchange, the pair may become a nearby pair for the same point. After determining the nearby pairs, we use analytical formula to calculate and superpose the interactive stress contribution of each nearby pair, and obtain the interactive stress for each simulation point. Since we only consider nearby TSV pair's contribution, the complexity of second stage is nearly irrelevant to the amount of TSVs for large designs but relevant to TSV integration density. However, since TSV integration density faces a upper bound in real applications, its influence on the run time of second stage also faces a limit. Therefore, the complexity of second stage mainly depends on the amount of simulation point and is linear in terms of it. Finally, we superpose the stress contribution calculated in the first and second stage, and obtain the stress analysis result.

5. Experimental Results

In this section, we validate the performance of proposed framework. We implement the linear superposition method and proposed framework in MATLAB. The golden result of stress analysis is generated by FEM simulation tool COMSOL [16]. The main material properties used in our modeling are as follows: Young's modulus (GPa) for copper = 110, BCB = 3, SiO2 = 71, silicon = 188; CTE (ppm/K) for copper = 17, BCB = 40, SiO2 = 0.5, silicon = 2.3. The radius of TSV body is 2.5um. The thickness of liner is 0.5um. And the dimension of landing pad is 6um.

5.1 Validation: A Placement of Two TSVs

We first validate the proposed framework in a placement containing two TSVs. In this placement, we vary the pitch between TSVs from 8um to 30um. Just as claimed by [17], the minimal pitch in the current process technology is 10um. However, since future TSV-based design will require higher TSV integration density to fully take advantage of the benefit of vertical integration, we validate the proposed framework in a broader range of pitch. Figure 4 compares the error of stress component σ_{xx} obtained by the linear superposition method and proposed framework under a 10um pitch. Due to symmetry, only right half analysis result is provided. Figure 4(a) shows linear superposition method leads to an error as much as 70MPa in some regions. Figure 4(b) shows the proposed framework can significantly alleviate the error of linear superposition method, and estimate the stress level around TSV with an error less than 25MPa generally.

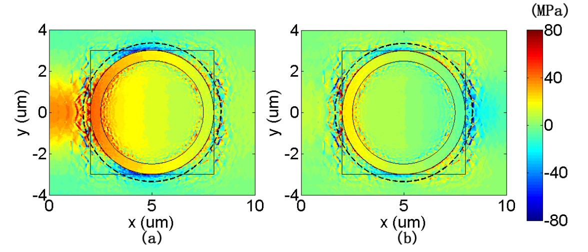

Figure 4. Comparison on the error of stress component σ_{xx} obtained by linear superposition and proposed framework for the placement of two TSVs (right half shot). (a) linear superposition method. (b) proposed framework.

	d (um)	Avg. Error (MPa)	Threshold 10MPa		Threshold 50MPa		Threshold 50MPa Critical Region	
			Avg. Error (MPa)	Avg. Error Rate(%)	Avg. Error (MPa)	Avg. Error Rate(%)	Avg. Error (MPa)	Avg. Error Rate(%)
LS	8	3.24	6.42	13.5	20.5	20.7	35.3	36.8
	9	2.63	5.35	11.3	16.0	16.1	27.6	28.9
	10	2.22	4.67	9.62	13.1	13.1	22.7	23.7
	11	1.90	4.16	7.99	10.9	10.9	19.4	19.9
	12	1.65	3.63	6.76	9.27	9.14	17.0	16.9
	18	0.92	1.88	3.20	4.82	4.84	10.4	8.58
	30	0.54	0.95	1.39	3.57	2.96	7.83	5.14
PF	8	1.96	4.01	8.94	11.7	11.0	16.0	14.3
	9	1.47	3.05	6.43	8.81	8.25	13.2	11.8
	10	1.19	2.58	4.85	7.35	6.78	11.8	10.4
	11	1.01	2.30	3.86	6.29	5.77	10.8	9.33
	12	0.89	2.07	3.28	5.57	5.04	10.1	8.48
	18	0.61	1.31	1.87	3.55	3.16	8.12	5.81
	30	0.47	0.87	1.12	3.44	2.77	7.64	4.97

Table 1. Comparison on the error of stress component σ_{xx} obtained by linear superposition and proposed framework for the placement of two TSVs. LS: linear superposition; PF: proposed framework.

Table 1 presents a quantitative comparison on the error of linear superposition method and proposed framework. Before we talk about this comparison, we need to define two concepts which facilitate the comparison. The first concept "monitored region" refers to the region which is influenced by TSV-induced stress to a certain extent. In this placement, we use a rectangular region as the monitored region. The center of monitored region is on the midpoint of the segment through the centers of two TSVs. Along x and y dimension shown in Figure 4, the dimensions of monitored region are respectively 60um and 30um. We use it as a baseline region of concern, and do the comparison listed in Table 1 in the monitored region except for the last two columns. The second concept "critical region" refers to the region influenced considerably by stress. We define it as the region within 3.3um to the center of each TSV, which is shown as the region within the dashed line around each of TSVs in Figure 4. The last two columns of Table 1 are the comparison for the critical region. We compare the linear superposition method and proposed framework in monitored region to give a general comparison on the stress estimation capability of two methods, while still compare them in the critical region which shows the difference on estimating stress in the region of more reliability concern. When we perform the comparison, we set a threshold on the stress intensity of simulation point, and only consider the point with intensity exceed the threshold. It is logical since only point with large stress intensity matters the reliability and mobility variation most, and thus should be emphasized.

Table 1 shows that the proposed framework considerably improves the accuracy of linear superposition method. For example, under the 8um pitch, the proposed framework can achieve a 14.3% average error rate for the stress component σ_{xx} in the critical region with 50MPa as threshold while the linear superposition method only achieve a 36.8% average error rate under the same condition. Since the interactive stress

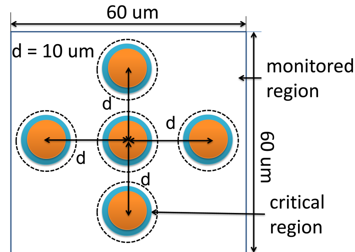

Figure 5. A placement of five TSVs.

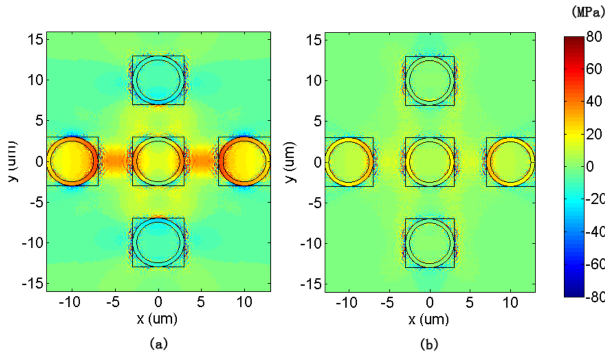

Figure 6. Comparison on the error of stress component σ_{xx} obtained by the linear superposition method and proposed framework for the placement of five TSVs. (a) linear superposition method. (b) proposed framework.

diminishes as the TSV pitch increases, linear superposition method and proposed framework achieve similar accuracy under the pitch of 30um. We also compare the run time of two methods, and find the proposed framework only takes around 1% additional run time compared to the linear superposition method. More results including the comparison on von Mises stress and comparison on the TSV structure with SiO2 liner are provided in Appendix A.2.

5.2 Validation: A Placement of Five TSVs

We also validate the proposed framework in a placement containing five TSVs shown as Figure 5. The minimal pitch is 10um in this placement. In this experiment, we also define monitored region and critical region. Since the placement has been changed, we slightly change the definition of monitored region in Section 5.1, and use a square region with dimension of 60um as the monitored region. We follow the previous definition of critical region, and the radius of each critical region is 3.3um. Figure 6 shows the comparison on stress component σ_{xx} obtained by linear superposition method and proposed framework. Figure 6(a) shows that linear superposition method leads to a stress error as high as 60MPa. While Figure 6(b) shows that the proposed framework generally ensures stress error within 25MPa. Table 5 shows the quantitative comparison on stress error obtained by the linear superposition method and proposed framework for this placement. We can see that the proposed framework significantly improves the accuracy of linear superposition method. For example, under the 50MPa threshold, the proposed framework achieves an average error rate of 12.6% and 8.22% respectively for the stress component σ_{xx} and von Mises stress in the critical region, while the linear superposition only achieves an error rate of 23.0% and 15.1% under the same circumstance. Though we use von Mises stress as a reliability metric here, since our proposed framework can achieve accurate stress tensor, it is also applicable to other reliability metric like maximum tensile stress. In the experiment, the proposed framework takes 4% additional run time compared to the linear superposition method.

6. Conclusions

In this paper, we have proposed the concept of interactive stress, analyzed its mechanism and characterized this stress using the complex variable method in elasticity. Based on the analytical solution to interactive stress, we have further proposed an accurate semi-analytical

	Stress Type	Avg. Error (MPa)	Threshold 10MPa		Threshold 50MPa		Threshold 50MPa Critical Region	
			Avg. Error (MPa)	Avg. Error Rate(%)	Avg. Error (MPa)	Avg. Error Rate(%)	Avg. Error (MPa)	Avg. Error Rate(%)
LS	σ_{xx}	2.84	5.45	11.6	13.9	13.1	22.8	23.0
	Von Mises	3.11	3.41	5.63	8.39	6.39	20.1	15.1
PF	σ_{xx}	1.60	3.05	5.74	8.19	7.19	13.8	12.6
	Von Mises	1.75	1.94	2.66	5.14	3.00	14.3	8.22

Table 2. Comparison on the stress error obtained by the linear superposition method and proposed framework for the placement consisting of five TSVs. LS: linear superposition; PF: proposed framework.

framework for full-chip TSV-induced stress modeling. Experimental results have demonstrated that the proposed framework can significantly reduce the error of linear superposition method with short additional run time. The remaining error of proposed framework is caused by the 2D nature of the analytical interactive stress model. Due to the generality of proposed framework, it can be applicable to TSV structures with various kinds of materials and geometry specifications. Therefore, we expect the proposed framework can be widely used in full-chip 3D IC reliability analysis and layout optimization.

7. Acknowledgment

This work is supported by NSF under Award No. 1018750 and SRC under Task No. 2238.001. The authors would like to thank Prof. Sung Kyu Lim from Georgia Tech and Dongjie Jiang from UT Austin for their helpful discussion.

References

[1] K. Athikulwongse, A. Chakraborty, J.-S. Yang, D. Z. Pan, and S. K. Lim, "Stress-driven 3D-IC placement with TSV keep-out zone and regularity study," in *Proc. ICCAD*, 2010.
[2] J. Yang, K. Athikulwongse, Y. Lee, S. K. Lim, and D. Z. Pan, "TSV stress aware timing analysis with applications to 3D IC layout optimization," in *Proc. DAC*, 2010.
[3] S.-K. Ryu, K.-H. Lu, X. Zhang, J.-H. Im, P. Ho, and R. Huang, "Impact of near-surface thermal stresses on interfacial reliability of through-silicon vias for 3-D interconnects," *IEEE Trans. Device and Materials Reliability*, vol. 11, no. 1, pp. 35 –43, 2011.
[4] M. Jung, X. Liu, S. Sitaraman, D. Z. Pan, and S. K. Lim, "Full-chip through-silicon-via interfacial crack analysis and optimization for 3D IC," in *Proc. ICCAD*, 2011.
[5] J. Zhang, M. Bloomfield, J.-Q. Lu, R. Gutmann, and T. Cale, "Modeling thermal stresses in 3-D IC interwafer interconnects," *IEEE Trans. Semiconductor Manufacturing*, vol. 19, no. 4, pp. 437 –448, 2006.
[6] C. Khong et al., "Numerical modeling of through silicon via (TSV) stacked module with micro bump interconnect for biomedical device," in *Proc. EPTC*, 2010.
[7] C. Zhang and L. Li, "Characterization and design of through-silicon via arrays in three-dimensional ICs based on thermomechanical modeling," *IEEE Trans. Electron Devices*, vol. 58, no. 2, pp. 279 –287, 2011.
[8] K. Lu, X. Zhang, S.-K. Ryu, J. Im, R. Huang, and P. Ho, "Thermo-mechanical reliability of 3-D ICs containing through silicon vias," in *Proc. ECTC*, 2009.
[9] M. Jung, J. Mitra, D. Z. Pan, and S. K. Lim, "TSV stress-aware full-chip mechanical reliability analysis and optimization for 3D IC," in *Proc. DAC*, 2011.
[10] M. Jung, D. Z. Pan, and S. K. Lim, "Chip/package co-analysis of thermo-mechanical stress and reliability in TSV-based 3D ICs," in *Proc. DAC*, 2012.
[11] J. Mitra, M. Jung, S.-K. Ryu, R. Huang, S. K. Lim, and D. Z. Pan, "A fast simulation framework for full-chip thermo-mechanical stress and reliability analysis of through-silicon-via based 3D ICs," in *Proc. ECTC*, 2011.
[12] C. Ko et al., "Structural design, process, and reliability of a wafer-level 3D integration scheme with Cu TSVs based on micro-bump/adhesive hybrid wafer bonding," in *Proc. ECTC*, 2012.
[13] Y. Chen, E. Kursun, D. Motschman, C. Johnson, and Y. Xie, "Analysis and mitigation of lateral thermal blockage effect of through-silicon-via in 3D IC designs," in *Proc. ISLPED*, 2011.
[14] N. Muskhelishvili, *Some Basic Problems of the Mathematical Theory of Elasticity*. Moscow: Nauka, 1966.
[15] S. Marella, S. Kumar, and S. Sapatnekar, "A holistic analysis of circuit timing variations in 3D-ICs with thermal and TSV-induced stress considerations," in *Proc. ICCAD*, 2012.
[16] COMSOL in *www.comsol.com*.
[17] G. Van der Plas et al., "Design issues and considerations for low-cost 3D TSV IC technology," in *Proc. ISSCC*, 2010.
[18] L. Yu, W.-Y. Chang, K. Zuo, J. Wang, D. Yu, and D. Boning, "Methodology for analysis of TSV stress induced transistor variation and circuit performance," in *Proc. ISQED*, 2012.

A. Appendix

A.1 Characteristics of Interactive Stress

1. The interactive stress between the aggressive and victim TSV has little influence on the stress distribution around aggressive TSV.

It is because interactive stress originates from the boundary of the victim, and has a similar stress level as the ideal stress distribution in that region. Suppose the stress level around the aggressive is N, according to [9], the level of ideal stress distribution around the victim will roughly be $N\left(R'/d\right)^2$, d is the pitch between TSVs, R' is the radius of TSV, $R'/d \leq 0.5$. Hence, the interactive stress has an intensity of $\alpha N\left(R'/d\right)^2$ around the victim. Since the interactive stress also decays with similar speed in the substrate, it will roughly decay to an negligible intensity of $\alpha N\left(R'/d\right)^4$ around the aggressive and thus have little influence on the stress distribution around the aggressive.

2. The interactive stress induced by the interaction of a TSV pair is nearly irrelevant to the existence of other TSVs nearby the pair.

Similar to the previous analysis, suppose the stress level around the aggressive is N , the interactive stress around the victim will be $\alpha N\left(R'/d\right)^2$. Suppose the distance between the victim TSV to the third TSV is also d , then the level of interactive stress around the third TSV will be $\alpha N\left(R'/d\right)^4$. Due to the mechanical property mismatch between the third TSV and substrate, the interactive stress will be changed around the third TSV, but the changes will still be in the similar level of $\alpha N\left(R'/d\right)^4$ and thus is negligible. Please note the interaction between victim TSV and the third TSV also induces interactive stress, but that is not a portion of interactive stress induced by the interaction between the original TSV pair.

A.2 Validation: More Results for the Case of Two TSVs

We employ von Mises yield criterion as a metric to access the reliability of 3D IC. Von Mises yield criterion determines whether a material starts to yield under a certain stress load. It can be calculated via

$$\sigma_v = \sqrt{\begin{array}{c}\frac{1}{2}(\sigma_{xx}-\sigma_{yy})^2+\frac{1}{2}(\sigma_{yy}-\sigma_{zz})^2+\frac{1}{2}(\sigma_{zz}-\sigma_{xx})^2 \\ +3(\sigma_{xy}^2+\sigma_{yz}^2+\sigma_{zx}^2)\end{array}}$$

Where σ_{xx}, σ_{xy}, σ_{xz}, σ_{yy}, σ_{yz} and σ_{zz} are stress components defined in Section 3.1. Please note that although von Mises yield criterion is used here, since our proposed framework can accurately calculate stress tensor, it is also applicable to other reliability metric like maximum tensile stress which is the maximum eigenvalue of stress tensor.

The comparison of von Mises stress obtained by linear superposition method and the proposed framework for the placement of two TSVs (Section 5.1) is given in Table 3. In this table, the definition of monitored region (column 3 - 7), critical region (column 8 - 9) and threshold is the same as those in Section 5.1. Table 3 shows that our proposed framework improves the accuracy of linear superposition method. For example, it improves the average error rate from 24.3% to 10.4% for the pitch of 8um case in the critical region under the threshold 50MPa.

We have demonstrated the performance of the proposed framework for TSV structure with BCB liner. As for SiO2 liner, we also compare the performance of linear superposition method and proposed framework for the placement of two TSVs, and list the comparison on stress component $\sigma_{xx}$and von Mises stress respectively in Table 4 and 5. The definition of monitored region (column 3 - 7), critical region (column 8 - 9) and threshold in these tables also follow those defined in Section 5.1. These tables show that linear superposition method can achieve acceptable accuracy. However, the proposed framework still improves the accuracy of linear superposition method. For example, it improves the average error of von Mises stress within critical region from 22.4MPa to 14.1MPa under the threshold of 50MPa in the case of 8um pitch.

	d (um)	Avg. Error (MPa)	Threshold 10MPa		Threshold 50MPa		Threshold 50MPa Critical Region	
			Avg. Error (MPa)	Avg. Error Rate(%)	Avg. Error (MPa)	Avg. Error Rate(%)	Avg. Error (MPa)	Avg. Error Rate(%)
LS	8	3.43	4.54	7.80	9.26	8.98	28.2	24.3
	9	2.62	3.41	5.95	7.15	6.33	20.6	15.6
	10	2.14	2.74	4.73	6.20	5.05	16.5	10.9
	11	1.81	2.29	3.87	5.42	4.21	14.3	8.25
	12	1.60	2.00	3.26	4.87	3.62	13.3	6.64
	18	0.98	1.14	1.64	2.85	1.83	10.8	3.70
	30	0.70	0.76	0.93	2.08	1.05	10.6	3.43
PF	8	2.22	2.91	3.98	6.73	5.59	17.3	10.4
	9	1.65	2.13	2.82	5.22	4.06	14.1	7.28
	10	1.34	1.73	2.16	4.56	3.22	12.5	5.69
	11	1.16	1.48	1.74	4.05	2.70	11.8	4.87
	12	1.06	1.34	1.46	3.76	2.36	11.6	4.42
	18	0.75	0.89	0.89	2.51	1.44	10.6	3.39
	30	0.64	0.70	0.77	2.00	0.95	10.6	3.42

Table 3. Comparison on the error of von Mises stress obtained by linear superposition and proposed framework for the placement of two TSVs. LS: linear superposition; PF: proposed framework.

	d (um)	Avg. Error (MPa)	Threshold 10MPa		Threshold 50MPa		Threshold 50MPa Critical Region	
			Avg. Error (MPa)	Avg. Error Rate(%)	Avg. Error (MPa)	Avg. Error Rate(%)	Avg. Error (MPa)	Avg. Error Rate(%)
LS	8	2.15	3.10	7.27	8.69	7.07	27.3	21.6
	9	1.75	2.55	5.91	7.12	5.63	21.7	17.0
	10	1.47	2.14	4.89	5.97	4.61	18.0	13.9
	11	1.26	1.84	4.13	5.12	3.88	15.6	11.7
	12	1.10	1.60	3.54	4.45	3.33	13.7	9.97
	18	0.62	0.97	1.57	2.58	1.97	8.66	5.68
	30	0.49	0.70	1.18	2.07	1.47	7.76	5.51
PF	8	1.99	3.15	6.77	8.80	7.32	14.6	10.1
	9	1.50	2.34	5.16	6.56	5.23	11.8	7.94
	10	1.17	1.81	4.05	5.07	3.94	10.0	6.64
	11	0.97	1.47	3.26	4.15	3.13	9.37	5.96
	12	0.81	1.23	2.68	3.43	2.56	8.57	5.40
	18	0.48	0.75	1.25	1.97	1.39	7.37	4.38
	30	0.47	0.63	1.11	1.88	1.27	7.20	4.94

Table 4. SiO2 liner: comparison on the error of stress component σ_{xx} obtained by linear superposition and proposed framework for the placement of two TSVs. LS: linear superposition; PF: proposed framework.

	d (um)	Avg. Error (MPa)	Threshold 10MPa		Threshold 50MPa		Threshold 50MPa Critical Region	
			Avg. Error (MPa)	Avg. Error Rate(%)	Avg. Error (MPa)	Avg. Error Rate(%)	Avg. Error (MPa)	Avg. Error Rate(%)
LS	8	2.19	2.31	3.03	4.51	3.29	22.4	12.5
	9	1.70	1.78	2.38	3.47	2.48	16.7	9.43
	10	1.38	1.43	1.92	2.84	1.93	13.1	7.16
	11	1.18	1.21	1.58	2.49	1.57	11.0	5.53
	12	1.03	1.06	1.33	2.30	1.36	9.48	4.34
	18	0.70	0.71	0.71	1.56	0.73	6.74	2.02
	30	0.66	0.68	0.69	1.25	0.63	6.40	1.82
PF	8	1.91	2.02	2.54	3.91	2.33	14.1	5.07
	9	1.51	1.58	1.93	3.15	1.87	11.2	3.94
	10	1.25	1.30	1.53	2.67	1.55	9.45	3.16
	11	1.09	1.12	1.25	2.42	1.35	8.47	2.66
	12	0.96	0.99	1.05	2.24	1.19	7.60	2.27
	18	0.68	0.68	0.57	1.58	0.75	6.49	1.86
	30	0.64	0.65	0.65	1.21	0.57	6.38	1.81

Table 5. SiO2 liner: comparison on the error of von Mises stress obtained by linear superposition and proposed framework for the placement of two TSVs. LS: linear superposition; PF: proposed framework.

Case #	1	2	3	4	5	6	7
TSV #	100	500	1000	100	100	100	100
TSV Density ($\times 10^{-2} \cdot \mu m^{-2}$)	1	1	1	0.69	0.25	1	1
Simulation Point #	0.5M	0.5M	0.5M	0.5M	0.5M	1M	2M
AR (%)	12	13	14	7.9	3.9	13	13

Table 6. Run time of the proposed framework. AR = additional run time of proposed framework / run time of linear superposition.

A.3 Run Time of the Proposed Framework

In order to examine the scalability of proposed framework, we run it on several placements which contain large amount of TSVs, and list the run time in Table 6. Case1, 2 and 3 show that AR (ratio of additional run time of proposed framework to the run time of linear superposition) nearly remains constant when the amount of TSVs increase. It accords with the theoretical analysis that both the run time of proposed framework and linear superposition method is irrelevant to the amount of TSVs. Case 1, 4 and 5 show that AR increases when TSV integration density increases. However, since the TSV integration density faces a upper bound in real application, the increase of run time due to the increase of TSV integration density also faces a upper bound. For example, in a very dense square TSV array with 10um pitch [18], the TSV integration density is only $1.0 \times 10^{-2} um^{-2}$. Hence, the TSV integration density in Case 1 approximates the upper bound but only makes AR as 12%. Case 1, 6 and 7 show that AR nearly remains constant when the amount of simulation points increases. It also accords with the previous theoretical analysis that both the run time of proposed framework and linear superposition method is linear with the amount of simulation points.

A.4 Constants & Functions

E_c, E_l and E_s , v_c, v_l and v_s, α_c, α_l and α_s are respectively Young's modulus, Poisson's ratio and CTE of corresponding materials, where subscript c, l and s respectively represent copper, BCB and silicon; T is the thermal load; R is the radius of TSV body; R' is the radius of TSV (including liner); $k = R/R'$.

$$K = -TR'^2 \left[\left(\tfrac{1-v_c}{E_c} + \tfrac{1+v_l}{E_l} \right) (\alpha_l - \alpha_s) + \left(\tfrac{1-v_c}{E_c} + \tfrac{1+v_l}{E_l} \right) (\alpha_c - \alpha_l) k^2 - \left(\tfrac{1-v_c}{E_c} - \tfrac{1-v_l}{E_l} \right) (\alpha_c - \alpha_s) k^2 \right] / \left[\left(\tfrac{1-v_c}{E_c} + \tfrac{1+v_l}{E_l} \right) \left(\tfrac{1+v_s}{E_s} + \tfrac{1-v_l}{E_l} \right) - \left(\tfrac{1-v_c}{E_c} - \tfrac{1-v_l}{E_l} \right) \left(\tfrac{1+v_s}{E_s} - \tfrac{1+v_l}{E_l} \right) k^2 \right]$$

$$a_1 = \left(1 + \frac{E_c}{E_l} \frac{3 - v_l}{1 + v_c} \right) / \left(1 - \frac{E_c}{E_l} \frac{1 + v_l}{1 + v_c} \right)$$

$$a_2 = \left(1 - \frac{E_c}{E_l} \frac{3 - v_l}{3 - v_c} \right) / \left(1 + \frac{E_c}{E_l} \frac{1 + v_l}{3 - v_c} \right)$$

$$G_1(m) = \frac{16 \left(k^2 - 1\right)^2}{E_l{}^2} + \left\{ \frac{4a_1 k^{2m+2} - 4}{E_l} + \left(\frac{1 + v_l}{E_l} - \frac{1 + v_s}{E_s} \right) \left[a_1 a_2 k^4 - a_1 k^{2m+2} - a_2 k^{2-2m} + \left(1 - k^2\right) \left(m^2 - 1\right) + 1 \right] \right\} \left\{ \frac{4a_2 k^{2-2m} - 4}{E_l'} + \left(\frac{1 + v_l}{E_l} + \frac{3 - v_s}{E_s} \right) \left[a_1 a_2 k^4 - a_1 k^{2m+2} - a_2 k^{2-2m} + \left(1 - k^2\right)^2 \left(m^2 - 1\right) + 1 \right] \right\} / \left(m^2 - 1\right)$$

$$G_2(m) = \frac{16}{E_l E_s} \left(1 - k^2\right) \left[a_1 a_2 k^4 - a_1 k^{2m+2} - a_2 k^{2-2m} + 1 + + (1 - k^2)^2 (m^2 - 1) \right]$$

$$G_3(m) = \frac{16 \left(k^2 - 1\right)^2}{E_l{}^2} + \left\{ \frac{4a_1 k^{2-2m} - 4}{E_l} + \left(\frac{1 + v_l}{E_l} - \frac{1 + v_s}{E_s} \right) \left[a_1 a_2 k^4 - a_1 k^{2-2m} - a_2 k^{2m+2} + \left(1 - k^2\right)^2 \left(m^2 - 1\right) + 1 \right] \right\} \left\{ \frac{4a_2 k^{2m+2} - 4}{E_l} + \left(\frac{1 + v_l}{E_l} - \frac{1 + v_s}{E_s} \right) \left[a_1 a_2 k^4 - a_1 k^{2-2m} - a_2 k^{2m+2} + \left(1 - k^2\right)^2 \left(m^2 - 1\right) + 1 \right] \right\} / \left(m^2 - 1\right)$$

$$F(m) = \begin{cases} G_2(m) / G_1(m), & \text{if } m \le -2 \\ G_3(m) / G_1(-m), & \text{if } m \ge 2 \end{cases}$$

$$F_1(m) = a_1 a_2 k^4 - a_1 k^{2m+2} - a_2 k^{2-2m} + 1 + \left(1 - k^2\right)^2 \left(m^2 - 1\right)$$

$$F_2(m) = \left(1 - k^2\right) (m + 1) F(m) + \left(a_2 k^{2-2m} - 1\right) (F(-m) + m + 1)$$

$$F_3(m) = \left(1 - k^2\right) (m + 1) (F(m) - m + 1) + \left(a_1 k^{2-2m} - 1\right) F(-m)$$

$$H(m) = \begin{cases} F_2(m) / F_1(m), & \text{if } m \le -2 \\ F_3(m) / F_1(-m), & \text{if } m \ge 2 \end{cases}$$

$$h_{11}(m) = (1 - a_2)(2 - m) H(m)$$

$$h_{12}(m) = (m - 1) + (a_1 - 1) k^{2-2m} H(-m) + (a_2 - 1) k^2 (m - 1) H(m)$$

$$h_{15}(m) = (1 - a_2)(2 + m) H(m)$$

$$h_{17}(m) = (1 - a_2) m H(m)$$

$$h_{13}(m) = h_{14}(m) = h_{16}(m) = h_{18}(m) = 0$$

$$h_{21}(m) = (2 - m) H(m)$$

$$h_{22}(m) = (m - 1) + (1 - m) k^2 H(m) + a_1 k^{2-2m} H(-m)$$

$$h_{23}(m) = (2 + m) H(-m)$$

$$h_{24}(m) = (m + 1) k^2 H(-m) + a_2 k^{2m+2} H(m)$$

$$h_{25}(m) = m H(m)$$

$$h_{26}(m) = m H(-m)$$

$$h_{27}(m) = (2 + m) H(m)$$

$$h_{28}(m) = (2 - m) H(-m)$$

$$h_{33}(m) = -(2 + m) F(m)$$

$$h_{34}(m) = F(-m) - (m + 1) F(m)$$

$$h_{36}(m) = (m - 2) F(m)$$

$$h_{38}(m) = -m F(m)$$

$$h_{31}(m) = h_{32}(m) = h_{35}(m) = h_{37}(m) = 0$$